Journal of Iron and Steel Research, International 24 (2017) 335－342

Contents lists available at ScienceDirect

Journal of Iron and Steel Research, International

journal homepage: www.chinamet.cn

Effect of hot/warm roll-forming process on microstructural evolution and mechanical properties of local thickened U-rib for orthotropic steel deck

Xue-feng Peng[1], Jing Liu[1,*], Jing-tao Han[1], Dong-bin Wei[2]

[1] School of Materials Science and Engineering, University of Science and Technology Beijing, Beijing 100083, China

[2] School of Electrical, Mechanical and Mechatronic Systems, Faculty of Engineering and Information Technology, University of Technology Sydney, Sydney 2007, NSW, Australia

ARTICLE INFO

Key words:
Orthotropic steel deck
Local thickened U-rib
Hot roll-forming process
Warm roll-forming process
Microstructural evolution
Deformation behavior

ABSTRACT

To improve the strength-toughness of traditional U-rib (TUR) and solve the problem of insufficient penetration between TUR and deckplate, a new local thickened U-rib (LTUR) has been proposed to improve the fatigue resistance of the weld joint under the premise of not increasing thickness and strength of the TUR material. And a hot/warm roll-forming process (RFP) adopting partially induction heating to 700－1000 ℃ was carried out to fabricate LTUR. The deformation behaviors in the forming process and microstructure of LTUR have been investigated. Mechanical properties and fracture mechanism of the LTUR after hot/warm RFP have been systematically discussed. Moreover, the results are compared with those obtained in cold RFP. Mechanical properties of the LTUR deformed above the critical transformation temperature (A_{c3}) show high performance characteristics with marked fatigue resistance and superior toughness. Upon increasing the heating temperature from 700 to 900 ℃, the initial coarse ferrite-pearlite structure transform into equiaxed ultrafine ferrite (1－3 μm) and precipitates such as (Nb,Ti)(C,N) are uniformly distributed in the matrix. The average dislocation density of the specimens after hot roll-forming at heating temperature of 900 ℃ decreases dramatically compared with those of the specimens subjected to the cold RFP. Furthermore, a typical characteristic of ductile fracture mechanism and the high impact energy are more convinced that the specimens deformed above 900 ℃ have obtained an optimal combination of strength and toughness.

1. Introduction

Since the middle of 20th century, the design level of steel box girder has been matured and the welding technique has been improved. The orthotropic steel deck system has been widely utilized for long-span steel bridges requiring light weight structures owing to its low depth, high strength and stiffness, easy processing and structural continuity[1]. This system consists of deckplate, crossbeams and U-ribs supporting the deckplate. Generally, the quantity of U-rib accounts for approximately 25% of the whole steel required of steel bridge design due to the high torsional stiffness and bending stiffness of U-rib[2]. Furthermore, it can effectively distribute an applied load on the deckplate. Therefore, U-rib is widely used in modern orthotropic steel deck system.

Orthotropic steel deck system belongs to thin-wall welding structure[3]. The welded joints between deckplate and U-rib in orthotropic steel deck system are potentially critical to fatigue failure due to stress concentration at the end of the weld toe[4]. The reason is the negative bending moments produced by live loads on the deck such as heavy weight trucks. Li et al.[5] pointed out that the fatigue cracks had often developed at welded connections of U-rib because of the large number of high magnitude axle loads, which lead to the fatigue life of orthotropic steel deck less than the designed service lifetime required by steel box girder. Wolchuk[6] suggested that the U-ribs should not be cut off and fitted between the floor beams. It is undoubted that transportation costs will increase and installation procedure will be more difficult. Xiao et al.[7] proposed to increasing the thickness and/or strength of U-rib material for reducing stress range and significantly increasing fatigue life of the welded joint. However, these methods exhibiting superior fatigue resistance have hardly been applied by bridge engineering for the reason

* Corresponding author. Prof., Ph.D.; Tel.: +86-10-62332752.
E-mail address: *liujing@mater.ustb.edu.cn* (*J. Liu*).

Received 21 July 2016; Received in revised form 26 October 2016; Accepted 1 November 2016
Available online 15 March 2017

of high costs. In addition, weight of bridge body will get greatly heavy if merely increasing the thickness of material.

The real reasons of fatigue cracks are that penetration depth is not sufficient because the welding process can only be implemented at the lateral side of U-rib and that the strength-toughness of traditional U-rib (TUR) material is low. According to the standards of AASHTO LRFD Bridge Design Specifications, Fatigue Design Recommendations for Road of Japanese, Design Specifications for Highway Bridges of Korean and Eurocode-3, the thickness and the penetration depth of U-rib are required not less than 8 mm and 80% of U-rib thickness, respectively. For the strength of U-rib material, 345 MPa grade steel widely used previously, such as SM490B, A572Gr50 or Q345qD, cannot meet the requirements of the development of steel box girder and is gradually replaced by a higher strength steel.

Studies[8-11] on enhancing the strength-toughness of metal by various methods to control the microstructure have been carried out. For high strength low alloy (HSLA) steel, grain refinement by means of plastic deformation at high temperature is feasible for producing excellent strength-toughness materials without any additive elements[12-15]. Hall and Petch[16,17] have explained the relationship between strength and average grain size by the Hall-Petch equation. Park et al.[18,19] proposed a heavy-reduction single-pass hot rolling process to enhance strength-toughness while the ductility was retained. They found that 0.2 wt.% carbon steel exhibited a superior combination between high strength and marked elongation after the plane-strain compression test above the critical transformation temperature A_{c3}. And the high-performance 0.2 wt.% carbon steel consisted of ultrafine or equiaxed fine grains with uniformly dispersed fine pearlite grains or cementite. The aim of this work is to present a processing technology for producing high performance U-rib with the similar above-mentioned microstructure at the edges without increasing thickness and strength of the whole TUR material. Moreover, the welding groove is improved. The microstructural evolution has been discussed in details via optical microscope (OM), field-emission scanning electron microscope (FE-SEM) and transmission electron microscope (TEM). More attention is paid to understand the relationship between mechanical properties and microstructure, precipitate as well as dislocation.

2. Experimental Procedure

2.1. Material and process

The investigated material, Q500qD, is a HSLA steel widely used in bridge engineering. According to Chinese standard GB/T 714-2008, the parent steel should have high strength-toughness, weldability and the ability of bearing loads and impact of vehicle. The chemical composition of the Q500qD steel is given in Table 1.

To solve the problem of insufficient penetration, a new U-rib structure is proposed for improving the fatigue resistance of the weld joint in this work, as shown in Fig. 1. And a hot/warm roll-forming process (RFP) model is developed to produce the local thickned U-rib (LTUR). This process model makes the microstructure and thickness of the LTUR edges different from other places instead of increasing the thickness and/or strength of the total U-rib material. Furthermore, the production costs of this new U-rib are not increased too much by replacing the traditional milling edges equipment using hot/warm roll-forming device.

Table 1
Chemical composition of investigated steel (mass%)

C	Si	Mn	P	S	Ti	Nb	Al
0.17	0.32	1.33	0.015	0.003	0.02	0.04	0.045

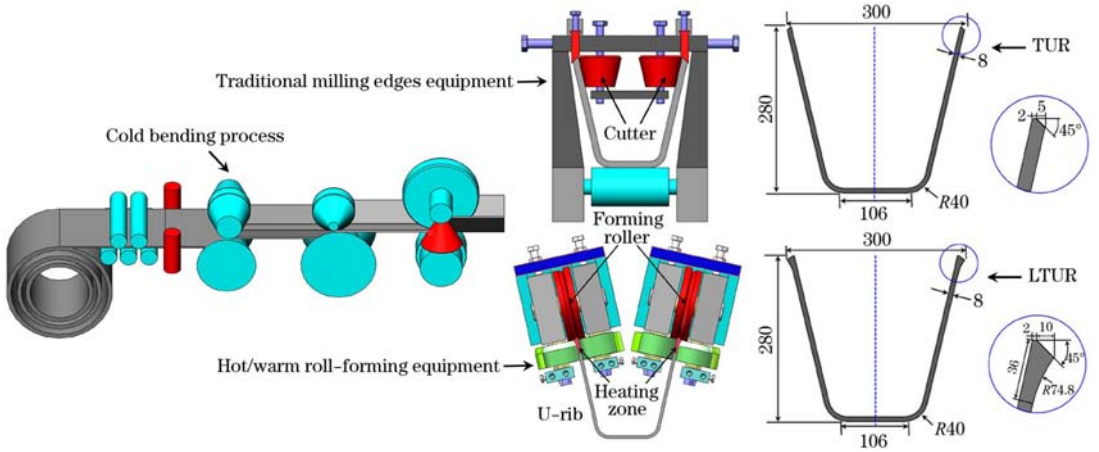

Fig. 1. Schematic diagram of traditional process and hot/warm RFP as well as sizes of TUR and LTUR (unit: mm).

A hot/warm RFP using induction heating was performed to produce the LTUR on the self-designed machine, as illustrated in Fig. 2. The experimental procedures used in the hot/warm RFP are presented in Fig. 3. The critical transformation temperatures A_{c1} and A_{c3} for Q500qD were calculated to be 718 and 841 ℃, respectively, adopting the empirical formulas of Andrews[20]. The specimens are heated to target temperatures of 700－1000 ℃ at a rate of 100 ℃/s by using an induction heating system after cold bending process. Then, the hot/warm RFP is performed at a rolling speed of 6.0 m/min according to requirements of customer. After roll forming, the specimens are cooled by air cooling.

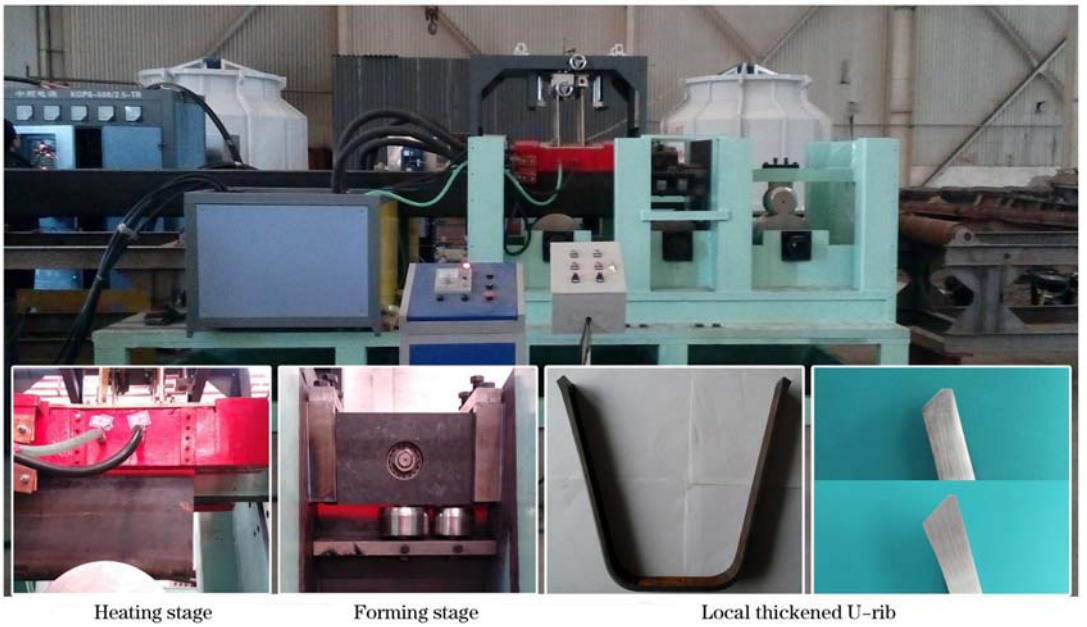

Fig. 2. Prototype of hot/warm RFP for LTUR.

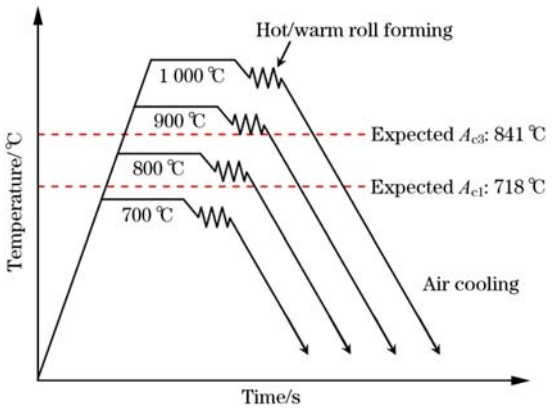

Fig. 3. Schematic diagram of experimental procedures in hot/warm RFP.

2.2. Mechanical properties testing

To evaluate the comprehensive mechanical properties of the edge of LTUR specimen, welding area measurement, flatting test, tensile test, microhardness test and Charpy V-notch impact test were performed. And the results were compared with those of the TUR and the cold roll-formed LTUR, respectively. The welding process between deckplate and U-rib applied CO_2 gas shielded arc welding. A CAD-software was used to calculate the weld area of the U-rib. Flattening tests were performed to indirectly indicate fatigue performance of specimen at room temperature on a universal testing machine of 200 kN capacity with a cross-head speed of 5.0 mm/min in accordance with Chinese standard GB/T 2653-2008. And tensile tests were conducted on the specimens at room temperature at a strain rate of 1×10^{-3} s^{-1} according to Chinese standard GB/T 228.1-2010. Vickers hardness tests were carried out with a load of 98 N on the basis of Chinese standard GB/T 4340.1-3009. Due to the size limitation of specimen, the Charpy V-notch impact specimens were machined with dimensions of 10 mm×7.5 mm×55 mm. An instrumented impact machine of 450 J capacity was used for Charpy impact tests at －20 ℃ according to Chinese standard GB/T 229-2007. Fracture surface characteristics of the broken tensile specimens after the tensile test were analyzed to achieve a better understanding of microscopic fracture mechanism.

2.3. Microstructure observation

The edges of specimens of cold, warm and hot RFP were etched in 4 vol. % nital solution after mechanical polishing, and the microstructures were observed by OM and FE-SEM. For further microstructure analysis, TEM observation was carried out using a FEI Tecnai G2 F20 TEM operated at 200 kV to ob-

serve microstructure, dislocation and precipitates (size, morphology and quantity). In addition, positron annihilation technique (PAT) was performed to analyze the variation in dislocation density of the U-rib edge. Positron source is ^{22}Na. The roll-formed specimens were machined into square plates of 20 mm× 20 mm, and the thickness was less than 1 mm after gently grinding of both sides in PAT test.

3. Results and Discussion

3.1. Mechanical properties

Fig. 4 gives the welding results. The effective welding areas of the TUR and the LTUR calculated by AutoCAD software are 24.85 and 66.80 mm^2, respectively. The effective welding area of the LTUR has increased to 2.45 times than that of the TUR. The thickness of U-rib partially thickened by hot/warm RFP actually became thicker than 8 mm. This means that the welding penetration, which has a great significant effect on the weld quality[21], becomes deeper. Thus, the hot/warm RFP can availably enhance welding penetration of the LTUR and improve fatigue resistance of the weld joint.

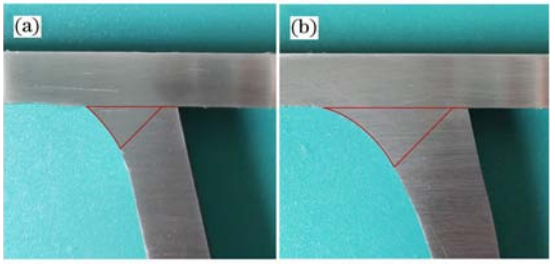

Fig. 4. Welding area of TUR (a) and LTUR (b).

Fig. 5 shows the loading model and the results of flattening tests for the cold, warm and hot roll-formed U-rib and the TUR. In the case of cold roll-formed LTUR, fatigue failure occurred early, and the value of compressive displacement was only 27.5 mm as seen in Fig. 5. It can also be seen that the load capacity has slightly decreased to less than 15 mm, which was caused by stress concentration during cold RFP. For the TUR and warm roll-formed LTUR, the yield occurred at 31.5 and 42.1 mm, respectively. Additionally, the specimen roll-formed at 700 ℃ can bear larger loading force than the traditional specimen. When the temperature of hot RFP was above 900 ℃, the yield did not occur again. However, the maximum loading capacity declined at 1000 ℃ indicated by the pink line in Fig. 5.

Fig. 6 shows the sampling position of tensile and impact specimens and the curves of mechanical properties with different roll forming temperatures. The

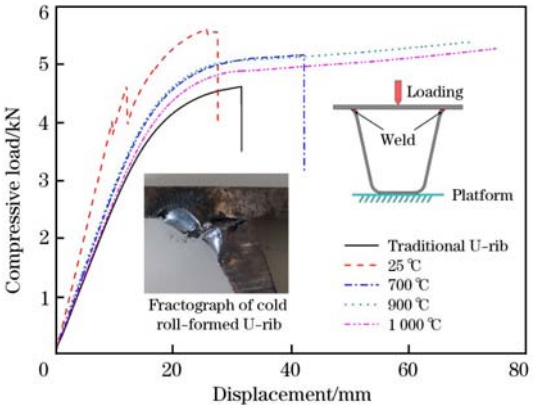

Fig. 5. Curves of flattening test of LTUR roll-formed at 25, 700, 900 and 1000 ℃ as well as TUR.

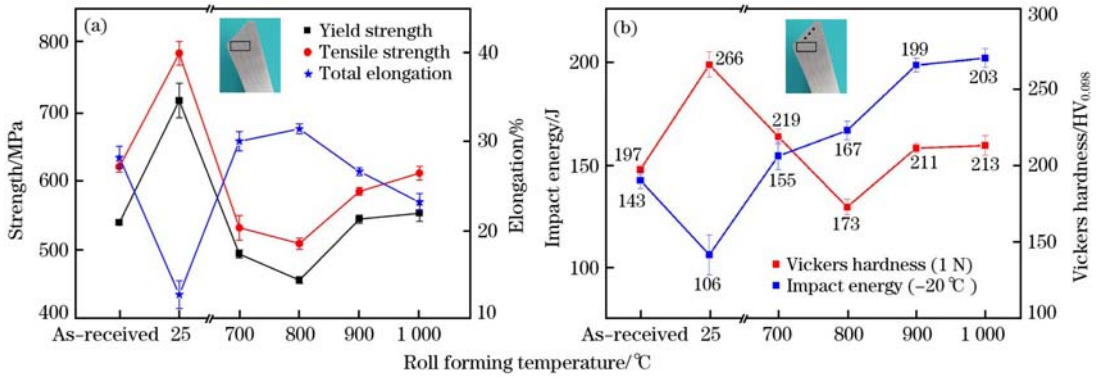

Fig. 6. Curves of mechanical properties versus different roll-forming temperatures.

tensile test results of the raw material indicated that tensile strength was 620 MPa and the total elongation was 27.7%. Compared with raw steel, the cold roll-formed specimen exhibited severe cold-hardening, which decreased the elongation value to 12.7% and increased the hardness value to 266 $HV_{0.098}$. The pinning effect caused by the increasing dislocation is the foremost factor in work hardening. When the forming temperatures were 700 and 800 ℃, the improvement of hardness value was mainly attributed to dynamic recovery and diffusion creep, with hardness value being 219 $HV_{0.098}$ and 173 $HV_{0.098}$, respectively. Although the elongation can be increased when warm roll-forming is adopted, the tensile

strength value is decreased to 532 and 509 MPa, respectively. However, when the roll-forming temperature is above 900 ℃, the tensile strength, yield strength and Vickers hardness values were slightly higher than those of the raw material.

The results of Charpy impact test in Fig. 6(b) are 75% of the value of standard specimen due to the size limitation of specimen. It can be seen that the roll-forming temperatures have a great influence on toughness of the specimen. When roll-forming at ambient temperature, impact energy dropped dramatically due to lots of tangled and pinned dislocations. At warm roll-forming temperature, impact energy got improved thanks to stress relief as well as disappearing of partial dislocations.

3.2. Microstructural evolution

The photographs obtained by OM, FE-SEM and TEM in Figs. 7－9 show microstructural evolution in the specimens after the various RFP. In Fig. 7 (a), the as-received steel consists of ferrite-pearlite structures with an average ferrite grain size of approximately 31 μm. Figs. 7(b) and 8(a) show that the grains subjected to cold RFP are elongated, and the grain size is smaller than the original average grain size. On the other hand, twins can be seen in Fig. 9(a). Twinning is one of the major deformation mechanisms in alloy steel, especially with low stacking fault energy, and at low deformation temperatures and high strain rates[22]. The microstructural component after roll-forming at heating temperatures of 700 and 800 ℃ is fine grains (8－10 μm) and uniformly distributed a bit of cementite as given in Figs. 7(c,d) and 8(b). The initial coarse ferrite-pearlite structure transformed into equiaxed ultrafine (1－3 μm) and finely dispersed pearlite or cementite structures in the matrix, and the ferrite grains were greatly refined after hot RFP at heating temperatures of 900 and 1000 ℃ above A_{c3} as seen in Figs. 7(e,f), 8(c) and 9(b). This result is in good agreement with the conclusion[18,19,23,24] that grain size became immensely decreased by the strain-induced transformation (γ-α) in various steels during thermo-mechanical treatment near A_{c3} or A_{r3}.

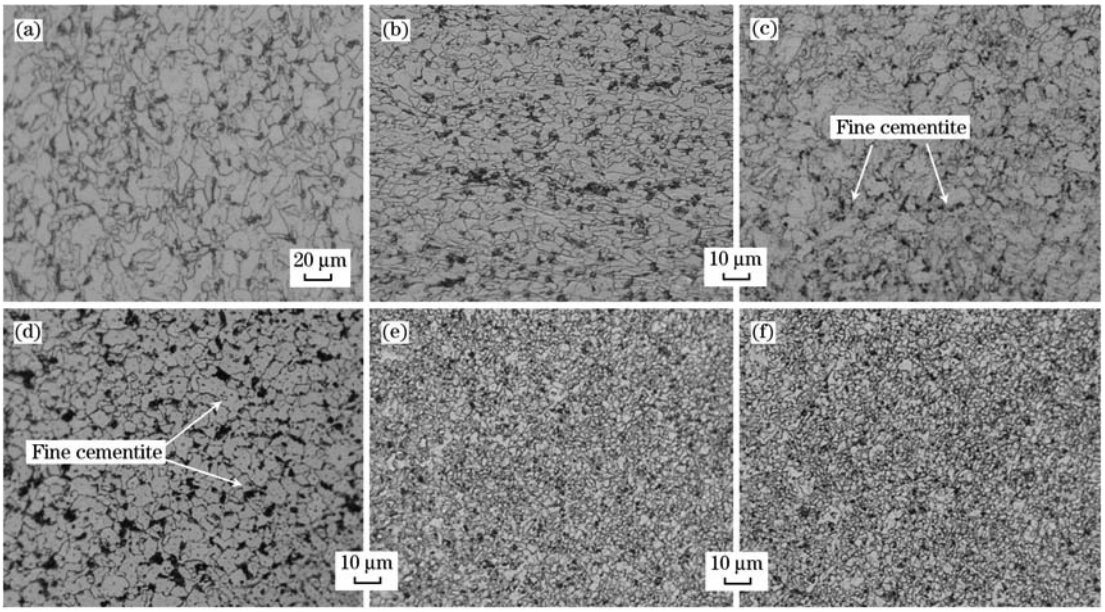

Fig. 7. Microstructures of deformation zone of LTUR roll-formed at as-received steel (a), 25 ℃ (b), 700 ℃ (c), 800 ℃ (d), 900 ℃ (e) and 1000 ℃ (f).

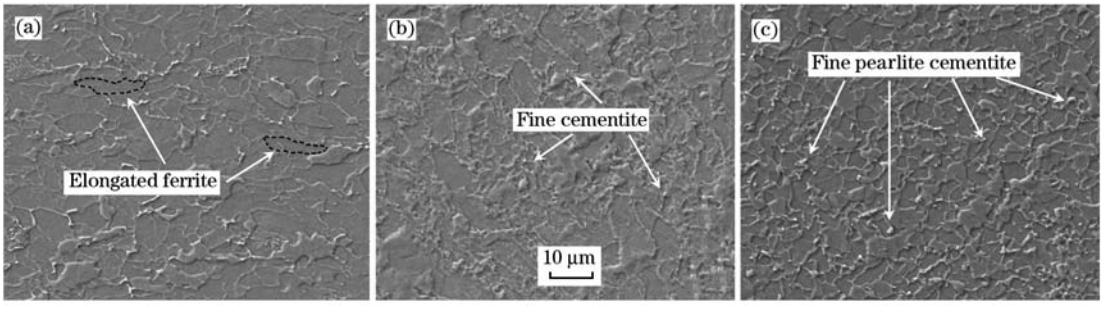

Fig. 8. FE-SEM micrographs of specimens subjected to RFP at temperatures of 25 ℃ (a), 700 ℃ (b) and 900 ℃ (c).

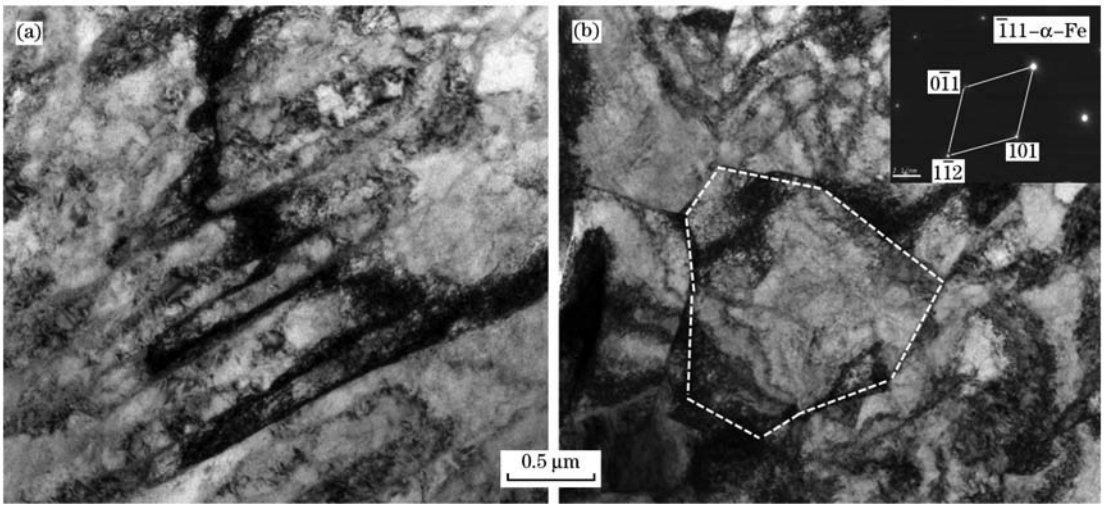

Fig. 9. Twins and equiaxed ferrite of specimens during RFP at temperatures of 25 ℃ (a) and 900 ℃ (b).

Fig. 10 shows TEM micrographs of precipitates in specimens roll-formed at temperatures of 900 and 1000 ℃. It is obvious that the amount of precipitates increases and they are more uniformly distributed with increasing the temperature. The sizes of these circular or elliptical precipitated particles range from 5 to 10 nm. The EDX analysis in Fig. 10(c) shows that these particles are precipitates of (Nb,Ti)(C,N). Because the heating and holding time was short so that precipitations had no time to grow up. This kind of precipitated particles formed in ferrite grains. Guo et al.[25] thought that these precipitates with sizes between 10—30 nm or even much smaller mainly contributed to precipitation strengthening, work hardening rate and microstructural stability. Carbide precipitation of Nb or Ti could give rise to toughness increasing at hot forming process of alloy steel[26]. This is the reason that strength and toughness further improved at forming temperatures of 900 and 1000 ℃ in Fig. 6.

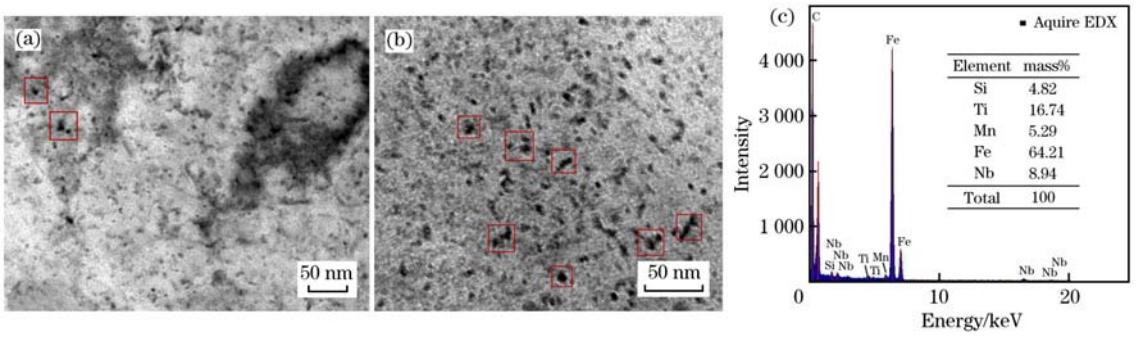

Fig. 10. TEM micrographs of precipitates in specimens treated by RFP at temperatures of 900 ℃ (a) and 1000 ℃ (b) and EDX analysis of precipitates (c).

3.3. Dislocation investigation

Fig. 11 presents the dislocation morphology of specimens experienced in RFP at temperatures of 25, 700 and 900 ℃. Fig. 12 gives the values of dislocation density under different RFP as well as the raw material acquired by PAT. From Fig. 11(a), it can be observed that dislocations mostly exist in form of dislocation package distributed in ferrite matrix or near grain boundaries. And the value of dislocation density of specimens at forming temperature of 25 ℃ is obviously higher than those of specimens at forming temperatures of 700 and 900 ℃ as shown in Fig. 12. The average dislocation density of specimen by cold roll-forming was 7.13×10^{15} m^{-2}, while the as-received steel was just 4.13×10^{13} m^{-2}. Although high dislocation density can enhance the strength of material, the plasticity and toughness decreased dramatically as seen in Fig. 6. At 700 ℃, the recovery including vacancy escape and ferrite polygon plays a great role in decreasing dislocation density. When roll-formed at 900 ℃, dislocation density shows a sudden drop in Fig. 12, which is related to stress release in the hot RFP of recovery and recrystallization. Irvine and Baker[27] thought that partial dislocation generated in the plastic deformation process

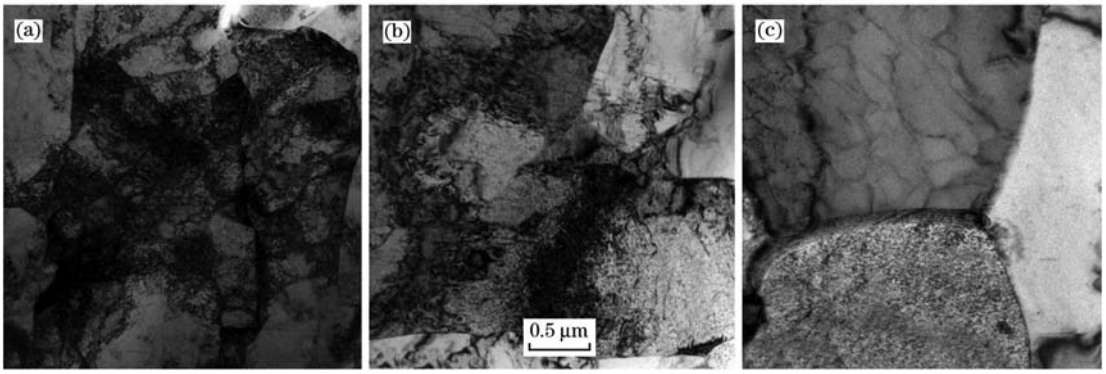

Fig. 11. Dislocation morphology evolution of specimens experienced to RFP at temperatures of 25 ℃ (a), 700 ℃ (b) and 900 ℃ (c).

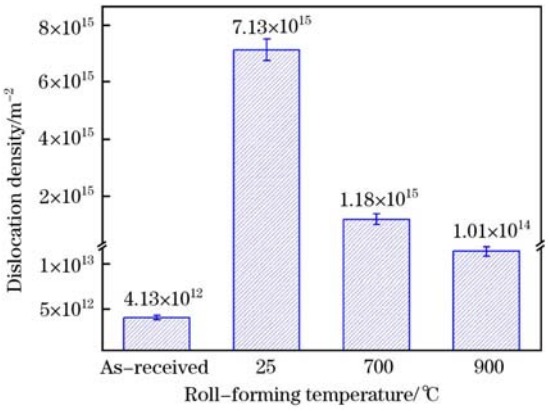

Fig. 12. Dislocation density under different RFP.

would disappear due to dislocation cross-slip and climb at high temperature deformation. And they found that the dislocation density decreased from 8×10^{13} m^{-2} to 5×10^{13} m^{-2} when the finish rolling temperature increased from 700 to 800 ℃.

3.4. Fractography

Fig. 13 shows scanning electron fractographs of the roll-formed specimens, which were taken to study the microscopic fracture mechanism of the specimens after the tensile test. As seen in Fig. 13(a), which gives the fractographs of the cold roll-formed specimens, facet fractures or cleavages of more than 10 μm represent brittle fracture, and numerous dim-

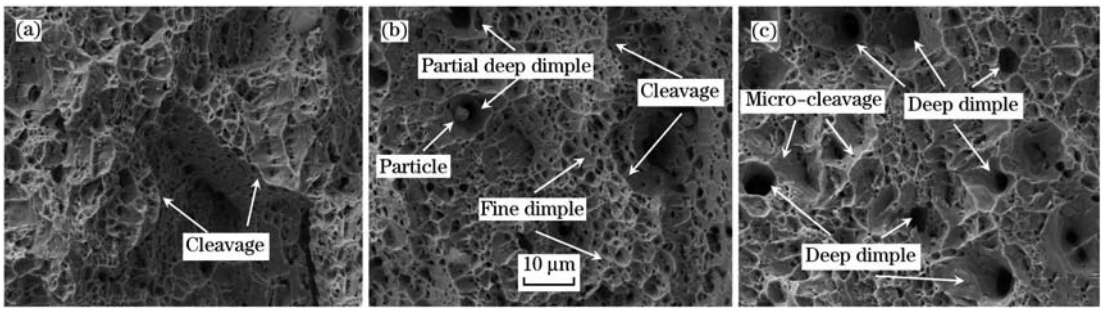

(a) 25 ℃; (b) 700 ℃; (c) 900 ℃.

Fig. 13. Fractographs of roll-formed specimens after tensile test.

ples reveal ductile fracture, covering the surface of each grain. In Fig. 13(b), the number of cleavages is decreased and the dimples become more and deeper when the deformation temperature increases from 25 to 700 ℃, which indicates ductile fracture with dimples of various sizes (1－10 μm). The different sizes dimples correspond to various void-nucleating mechanisms on the fracture surface. The small dimples mainly originate from fine carbonitride particles precipitated in the matrix. Due to the low bonding force between the fine precipitated phases and the relatively soft matrix, the micro-voids readily form in the interfaces during tensile text. On the other hand, the large dimples mainly result from inclusion particles. The micro-cleavage fractures in Fig. 13(c) and the deep dimples with a diameter of about 10 μm can be locally seen in a matrix of dimples of less than 2 μm in diameter, which is commensurate with the high strength-toughness in Fig. 6 obtained by mechanical performance testing.

4. Conclusions

(1) Compared with the TUR, the LTUR had distinctly improved welding penetration. Concerning the fatigue resistance and strength-toughness, the cold roll-formed LTUR was more sensitive to the fa-

tigue test and Charpy V-notch impact test, while the LTUR after hot RFP achieved high mechanical properties. The characteristic of ductile fracture and high impact energy were more convinced that the specimen after hot RFP obtained an optimal combination of strength and toughness.

(2) The initial coarse ferrite-pearlite structure of raw material transformed into equiaxed ultrafine ferrite (1—3 μm) and finely pearlite and cementite structures dispersed in the ferrite matrix, and the ferrite grains were greatly refined after hot RFP at heating temperatures of 900 and 1000 ℃. A large number of finely dispersed carbonitride precipitates got the toughness further improved.

(3) The reduction of dislocation density of investigated steel after hot roll-forming weakened the trend of dislocation pile-up and internal stress concentration due to dislocation cross-slip and climb at elevated temperature deformation, which are beneficial for toughness.

Acknowledgment

The authors would like to gratefully acknowledge the help of Dr. Mustapha Boukhir in the final language editing of this paper.

References

[1] R. C. Battista, M. S. Pfeil, E. M. L. Carvalho, J. Constr. Steel Res. 64 (2008) 134-143.
[2] P. P. Xanthakos, Theory and Design of Bridges, New York, USA, 1994.
[3] C. K. Oh, K. J. Hong, D. Bae, H. Do, T. J. Han, Int. J. Steel Struct. 11 (2011) 227-234.
[4] D. H. Choi, D. H. Kim, J. H. Choi, D. I. Chang, J. Korean Soc. Steel Constr. 11 (1999) 559.
[5] M. Li, K. Hashimoto, K. Sugiura, J. Bridge Eng. 19 (2014) 04014038.
[6] R. Wolchuk, J. Struct. Eng. 116 (1990) 75-84.
[7] Z. G. Xiao, K. Yamada, S. Ya, X. L. Zhao, Int. J. Fatigue 30 (2008) 1387-1397.
[8] T. J. Rupert, J. C. Trenkle, C. A. Schuh, Acta Mater. 59 (2011) 1619-1631.
[9] D. N. Seidman, E. A. Marquis, D. C. Dunand, Acta Mater. 50 (2002) 4021-4035.
[10] D. A. Terentyev, G. Bonny, L. Malerba, Acta Mater. 56 (2008) 3229-3235.
[11] M. J. Alinger, G. R. Odette, D. T. Hoelzer, Acta Mater. 57 (2009) 392-406.
[12] R. Song, D. Ponge, D. Raabe, R. Kaspar, Acta Mater. 53 (2005) 845-858.
[13] T. K. Lee, C. H. Park, D. L. Lee, C. S. Lee, Mater. Sci. Eng. A 528 (2011) 6558-6564.
[14] K. Hanazaki, J. Tokutomi, J. Yanagimoto, N. Tsuji, Mater. Sci. Eng. A 534 (2012) 720-723.
[15] Y. Estrin, A. Vinogradov, Acta Mater. 61 (2013) 782-817.
[16] E. O. Hall, Proc. Phys. Soc. B 64 (1951) 747-753.
[17] N. J. Petch, J. Iron Steel Inst. 174 (1953) 25-28.
[18] H. W. Park, J. Yanagimoto, Mater. Sci. Eng. A 607 (2014) 542-550.
[19] H. W. Park, K. Shimojima, S. Sugiyama, H. Komineb, J. Yanagimoto, Mater. Sci. Eng. A 624 (2015) 203-212.
[20] G. Krauss, Principles of Heat Treatment of Steel, American Society for Metals, Ohio, 2005.
[21] I. S. Kim, J. S. Son, I. G. Kim, J. Y. Kim, O. S. Kim, J. Mater. Process. Technol. 136 (2003) 139-145.
[22] J. W. Christian, S. Mahajan, Prog. Mater. Sci. 39 (1995) 1-157.
[23] R. Song, D. Ponge, D. Raabe, J. G. Speer, D. K. Matlock, Mater. Sci. Eng. A 441 (2006) 1-17.
[24] K. Nagato, S. Sugiyama, A. Yanagida, J. Yanagimoto, Mater. Sci. Eng. A 478 (2008) 376-383.
[25] A. Guo, R. D. K. Misra, J. Q. Xu, B. Guo, S. G. Jansto, Mater. Sci. Eng. A 527 (2010) 3886-3892.
[26] V. C. Olalla, V. Bliznuk, N. Sanchez, P. Thibaux, L. A. I. Kestens, R. H. Petrov, Mater. Sci. Eng. A 604 (2014) 46-56.
[27] J. Irvine, T. N. Baker, Mater. Sci. Eng. 64 (1984) 123-134.